Etching of Fission Tracks in Monazite: Further Evidence from Optical and Focused Ion Beam-Scanning Electron Microscopy

Sean Jones, Barry Kohn, Andy Gleadow

School of Geography, Earth and Atmospheric Sciences, University of Melbourne, Victoria 3010, Australia

Abstract

A series of experiments on monazites from Victoria, Australia are presented to further understand their fission track etching properties. Using a 6M HCl etchant at 90°C, SEM images on crystal (100) pinacoid faces reveal well-etched rhombic spontaneous fission track openings. Average rhombic etch pit diameters Dpc and Dpb, parallel to the crystallographic *c*- and *b*-axes are 0.81 ± 0.20 μm and 0.73 ± 0.26 μm, respectively. An angular distribution experiment on (100) faces found that spontaneous fission tracks initially etch anisotropically, being preferentially revealed at an azimuth of 90° to the crystallographic *c*-axis up to ~60 min of etching. As etching continues, however, the distribution becomes progressively more uniform and is essentially isotropic by 90 min. Two experimental methods determined the rate at which the etchant penetrated along the lengths of implanted ^{252}Cf fission tracks. This involved the application of a focused ion beam scanning electron microscope (FIB-SEM) to mill progressively into slightly etched monazite crystals followed by an etch-anneal-etch approach. Results indicate that at least the greater part of the etchable ranges of the latent fission tracks were penetrated by the 6M HCl etchant

within the first few min. Continued etching to 5 min indicates that track etching slows down towards the ends of the tracks, but the maximum ranges are estimated to be reached after 5 – 15 min, which represent the longest time the latent segments of the tracks are exposed to potential annealing at the etchant temperature. Taking into account that implanted ^{252}Cf fission tracks in monazite anneal on average ~4% of their length at 90°C after 1 hour (Jones et al., 2019), suggests that a much shorter duration for exposure to this temperature causes less than ~1% of fission track length reduction during etching.

Keywords: Monazite, fission tracks, etching, FIB-SEM, etch-anneal-etch.

1. Introduction

A series of experiments presented by Jones et al. (2019) led to a first-order understanding of monazite fission track etching properties. An alternative 6M HCl (1:1 HCl (37%): H_2O by volume) etchant at 90°C for 60 – 90 min was introduced, rather than using concentrated 37% HCl (12M) at 90°C for 45 min (originally proposed by Shukoljukov & Komarov (1970). The weaker etchant proved to reduce both grain corrosion and grain loss from epoxy mounts, while still producing well-etched fission tracks. Results from an electron backscatter diffraction (EBSD) experiment demonstrated that when using standard mounting techniques (see Kohn et al., 2019 for procedure), the majority of euhedral grains would settle on their (100) pinacoid faces as the dominant orientation. A 90°C isothermal annealing experiment illustrated the degree of track length reduction of implanted ^{252}Cf fission tracks under laboratory timescales. This experiment also demonstrated the low temperature sensitivity of fission tracks in monazite, with a total of ~4% annealing occurring after one hour, and a maximum of ~20% reduction after 15 hours. The final experiment of the study indicated that there is some compositional control (principally by U and Th) on track etching rates between different monazite grains, suggesting that there is a weak relationship with accumulated radiation damage.

These experiments were an important first step towards understanding the etching characteristics of fission tracks in monazite, however further information is required to establish a standardized protocol for track etching and measurement. It is evident from earlier studies that tracks in monazite undergo substantial annealing at relatively low temperatures (e.g. Weise et al., 2009), thus a key concern is the question of the degree of track annealing that occurs using the 6M HCl etchant at 90°C on laboratory timescales. The question also arises as to the rate of etchant penetration along the length of tracks. In one of the earliest track etching experiments, Price & Walker (1962) demonstrated that etchants penetrate almost instantaneously along the highly reactive core of latent tracks in mica. Observations made by transmitted electron microscopy showed that well-defined hollow channels in various micas appeared in <1 second. Recent experiments in apatite also found that in the earliest stages, the etching rates of both latent spontaneous and induced fission tracks in apatite are significantly higher at their cores (Tamer & Ketcham, 2020). A similar relationship might be assumed to occur in other minerals, including monazite, meaning that the actual exposure of annealable latent tracks to 90°C before they are etched is most likely negligible, and certainly much less than the ~4% shortening that would result if the latent tracks had been annealed over the entire duration of etching.

In this study, using implanted ^{252}Cf fission tracks, we quantify the size and shape of well-etched spontaneous fission track openings in monazite, giving an indication of the typical shape and dimensions to expect on surfaces parallel to the (100) plane. A well-etched fission track has been defined as being entirely etched to the track termination point. Criteria taken into consideration are observing the track itself to be well developed in width and consistently tapering to its termination point, which is generally rounded in form. Using the same crystal orientation, the results of an angular distribution experiment are also presented, illustrating the rate at which spontaneous fission tracks are revealed in different directions. Lastly, we assess the rate at which the 6M HCl etchant penetrates along the length of the highly reactive latent track cores. This is achieved with the application of a focused ion beam scanning electron microscope (FIB-SEM), which mills into partly etched monazite crystals and allows measurement of the widths and lengths of implanted tracks after short etching times of 10 and 15 min. These results are then complemented with an etch-anneal-etch approach (Tamer & Ketcham, 2020) to measure implanted track lengths after two very short etching times of 1 and 5 min.

2. Experiments and Results

Monazite crystals from the late Devonian, high-K, calc-alkaline Harcourt Granodiorite (Victoria, Australia) were used throughout this study (Clemens, 2018). These euhedral crystals range from ~100 – 250 μm in length and are classified as Ce dominant (Jones et al., 2019). An additional sample mount containing well-formed alluvial monazite crystals from Beechworth (Victoria, Australia) was also analysed in Section 2.1. This sample was obtained by the Cocks Eldorado Dredge in the gold-rich alluvial sediments of Reedy Creek between 1940 – 1942 (Sullivan, 1947). The crystals range from ~75 – 200 μm in length and are also characterized as Ce dominant (Table 1). The conditions and methods used in the experiments reported in this study are summarized in Table 2.

2.1 Track Etch Pits

To constrain the size and shape of well-etched spontaneous fission tracks in monazite, the diameters of the track etch pits were measured manually using both optical and scanning electron microscopy (SEM) on two separate monazite mounts (Table 3).

Each mount contained 48 monazite crystals which were positioned manually on their (100) pinacoid faces using double-sided tape. The grains were then mounted in cold-setting *Struers* Epofix epoxy, slightly ground using a *Struers* MD-Piano 1200 grinding disc and finally polished using 6, 3, 1 and 0.25 μm diamond pastes. Both samples were then etched in 6M HCl at 90°C for 75 min. A thin gold coating was then applied using a sputter coating unit, which reduced internal reflections under the optical microscope and added a conductive layer for SEM imaging. Digital images of all monazite grains in each mount were captured in reflected and transmitted light using a 100x dry objective on a *Zeiss* Axio Imager M1m motorized microscope fitted with a *PI* piezo-motor scanning stage and a 4 Megapixel IDS μEye USB 3 CMOS digital camera. This was interfaced to a control PC using *TrackWorks* software Version 3.1.10 (Gleadow et al., 2009; Gleadow et al., 2019).

New terminology is introduced here to describe the dimensions of track etch pits in monazite (Figure 1). These are described as Dpc and Dpb (diameter of track etch pits parallel to crystallographic *c*- and *b*-axes, respectively), which are equivalent to the more familiar parameters Dpar and Dper (track diameters parallel and perpendicular respectively to the *c*-axis, Donelick et al., 2005) used to describe the track pit dimensions in uniaxial minerals such as apatite and zircon. Both Dpc and Dpb measurements were made manually from the captured reflected light image stacks on a separate computer using *FastTracks* software Version 3.1.10 (Gleadow et al., 2009; Gleadow et al., 2019).

Grains identified with well-etched fission tracks in *FastTracks* were also measured on a JEOL JXA-8530F Field Emission Electron Probe Microanalyzer (EPMA) using its SEM imaging mode. The operating software on this analytical instrument also allowed high resolution SEM images of the track etch pits to be captured, and their dimensions measured using the ruler tool.

Table 3 presents average Dpc and Dpb optical (FastTracks, 15,000x on-screen magnification) and SEM measurements (11,000 – 33,000x) for well-etched spontaneous fission track openings in monazite. The two diameter measurements were made on the same etch pits, but it was not always possible to confidently measure both Dpc and Dpb in every case optically, so that the total numbers are different. The ability to view the etch pits at much higher magnifications on the SEM allowed both Dpc and Dpb measurements to be made on exactly the same etch pits in all cases, resulting in the same numbers for each. The same grains were chosen for analysis for both the optical and SEM measurement, but it is not known if the exact same etch pits were measured by the two modes.

All measurements across the two samples are broadly similar in size, and, with one exception, the optical and SEM measurements are in close agreement. The greatest difference is for the Dpb parameter in the Eldorado monazite (~0.11 μm), possibly due to the much smaller number of measurements made on the SEM. It is worth noting that neither Dpc nor Dpb are on average consistently larger than the other across both mounts.

2.2 Angular Distribution

Twenty-five monazite crystals from the Harcourt Granodiorite were positioned manually on their (100) faces using double-sided tape, then mounted, ground and polished as described in Section 2.1. The mount was then progressively etched using the 6M HCl etchant at 90°C for times of 20, 40, 60 and 90 min. Between each progressive etching step, images were captured on the same grains in both reflected and transmitted light. Spontaneous fission track lengths and azimuth angles relative to the c-axis were manually measured on the captured image stacks using *FastTracks* software (Gleadow et al., 2009; Gleadow et al., 2019). The digital image stacks allowed exactly the same individual tracks to be measured after each etching step as well as additional tracks that were revealed as etching progressed. The surface reflected light image was used to manually determine the centers of the spontaneous track etch pits, and the transmitted light stack for determining the position of track terminations. Track ends were determined by scrolling down through the transmitted light image stack and stopping at the termination point in the last image plane where it appeared clearly in focus. Defining the direction of the crystallographic *c*-axis allowed *FastTracks* to automatically record the track azimuth angles.

Results of the angular distribution experiment are presented in Figure 2. It is evident that spontaneous fission tracks are strongly anisotropic in the early stages of etching. Tracks with azimuths perpendicular to the *c*-axis are revealed more quickly than those oriented parallel to it. As etching proceeds, however, relatively more tracks are revealed parallel to the *c*-axis than perpendicular, so that the degree of anisotropy progressively decreases until etching appears to be essentially isotropic by 90 min. This can be seen in the ratio of the Number of tracks from 75-90° to the c-axis relative to the number from 0-15° in each case ($N_{75\text{-}90}/N_{0\text{-}15}$ in Fig. 2c). Over-etching of the tracks as well as increased track density makes measurement more challenging after 90 min, causing the total number of measured tracks to decrease slightly than in the earlier stages of the experiment (Figure 2b).

2.3 Etchant Penetration

Eight pre-annealed (400°C for 8 hours) Harcourt Granodiorite monazite crystals were manually oriented on their (100) faces using double-sided tape for each of one control and five sample mounts. Samples were then mounted, lightly ground and polished as described in Section 2.1, followed by irradiation under vacuum for 30 hours with collimated fission fragments from a ^{252}Cf source. Implanted ^{252}Cf fission tracks were used for this experiment to enable control of both track density and orientation. Additionally, ^{252}Cf fission fragments have a similar mass distribution to those of ^{238}U, and therefore serve as a useful proxy for the etching of ^{238}U fossil tracks (Wagner & Van den Haute, 1992). The fission tracks were implanted at a dip angle of approximately 30° to the sample surface. Each sample mount was then etched for a different time of 60 (control), 15, 10, 5 and 1 min in 6M HCl at 90°C.

In preparation for the FEI Nova Nanolab dual beam scanning electron microscope (FIB-SEM), located at the Melbourne Advanced Microscopy Facility, each sample mount was then carbon coated and carbon tape attached. A background summary of the FIB-SEM system is given by Wirth, (2009) and Young & Moore, (2005). The coated mount was attached to the FIB-SEM sample holder and raised to the eucentric height where the beam focus, stage tilt axis and sample feature of interest intersect. The sample was tilted to 52° to allow the FIB to penetrate perpendicular to the surface and both ion and electron beams were focused on exactly the same spot on the sample surface. This geometry meant that the electron beam for observation was facing the surface at 30°, the same angle at which the ^{252}Cf tracks were implanted. Thus, as the subsurface was milled back the same etched tracks could be followed from the surface to their ends.

Suitable areas on grains were then chosen for analysis where fission tracks had been identified and no cracks were present. Using the gas injection system (GIS) and assistance of the FIB, sample surfaces of interest were then coated with platinum, typically in sets that had dimensions of 25 μm x 2 μm x 1 μm (W x L x H) using settings of 30Kv and an aperture of 0.30 nA. The platinum deposit is used to protect the area of interest from damage during the long process of ion milling and imaging. Up to 10 platinum sets were deposited and trenches around the area of interest were milled out of the sample, typically to 3.5 μm in depth. The trenches produced a 'U' shape and were important because they isolated the area of interest, provided space for milled material to be redeposited and lowered the chance for milled material to settle on the sample face of interest. The FIB settings for trench milling were 7.0 nA (aperture) and 30 kV. Once the trenches were milled, analysis of the sample could begin. Cross-sections of 25 μm x 1 μm x 3.5 μm (W x L x D) were milled through the sample face of interest, with FIB settings of 1 nA and 30 kV. Milling at 1.0 nA was slower, but produced a cleaner slice and ensured that clear analysis of the ion milled subsurface was possible. Figure 3 illustrates a cross-section of the experimental setup as well as a supporting SEM image of milled monazite with etched ^{252}Cf fission tracks from the control sample of the experiment.

This is the peer-reviewed, final accepted version for American Mineralogist, published by the Mineralogical Society of America.
The published version is subject to change. Cite as Authors (Year) Title. American Mineralogist, in press.
DOI: https://doi.org/10.2138/am-2022-8002. http://www.minsocam.org/

Eight live images of the implanted tracks on the milled surface were integrated to produce a single high resolution (1024 x 884) still image. For each image the horizontal diameter (~Dpb) and depth below the original surface (contact with platinum, Fig. 3b) were recorded. Typically, about 500 tracks were measured for each sample on ~360 images captured over ~34 milled planes. All measurements were automatically corrected for tilt on the FIB-SEM software. By measuring the depth of the tracks within the sample and knowing the implantation angle (30°) allowed simple geometry to be applied and determine at what distance along the length of the etched fission tracks the measurements were recorded.

Table 4 and Figure 4 present the average ^{252}Cf fission track width parameter Dpb for continuous increments down the track lengths for different etching times of 60 (control), 15 and 10 min. A total of 529 fission track widths were measured for the 60 min control sample, which overall show decreasing track widths along the track lengths towards the termination. However, platinum was able to penetrate ~1.50 μm and deposit on the walls of some of the etched track openings (Figure 5), resulting in smaller Dpb measurements near the surface that did not represent their true widths during the earliest stages of ion milling. This was particularly prevalent in the control sample, where the larger tracks allowed more space for the platinum to penetrate. As a result, these early measurements for the 60 min dataset are plotted separately and excluded from the trend line in Figure 4. A similar effect is not observed in the 15 and 10 min datasets due to the much smaller diameter of their track openings. The maximum track length recorded in the 60 min control sample was between 8.01 - 8.50 μm.

Tracks etched for 15 min showed a similar overall decreasing width along the track lengths, averaging 55.6 ± 6.7 nm across 216 analyses and decreasing from a near-surface average of ~84 nm to an ~36 nm at a distance of 4.5-6.0 μm along the track (Figure 4). A total of 553 widths were recorded after a 10 min etch, averaging 33.7 ± 6.6 nm in diameter across all analyses. The tracks show an overall trend of decreasing average width from ~47 nm near the surface to ~23 nm at lengths between 6.5–7.0 μm. No track widths were measurable beyond these lengths but evidence of the continued presence of etched tracks was observed at lengths up to 8.5-9.0 μm in the 15 min sample. Track openings on the surface in the 15 and 10 min etching experiments show a larger Dpb than the subsurface widths, recorded as 104.1 ± 15.8 nm and 73.2 nm respectively, suggesting some flaring of the track openings.

Table 4 and Figure 6 show the percentage of tracks measured at different increments along the lengths of the implanted fission tracks. In the 60 and 15 min experiments, the highest percentage of tracks measured was between 1.01 – 1.50 μm. The 10 min experiment showed the highest percentage of tracks measured is between 2.01 – 2.50 μm, followed very closely by the 1.01 – 1.50 increment at 12.5% and 12.1%, respectively. Each etching experiment followed a similar trend, decreasing in the number of measured fission tracks, and ending at a maximum length between 8.51 – 9.00 μm in the 15 min etch schedule. The 60 min control sample had a maximum width measured between 8.01 – 8.50 μm along the track and the 10 min etch had a maximum width measured between 6.51 – 7.00 μm. Only the 15 min etching schedule produced gaps in the data between length increments of 6.01 – 6.50 μm and 7.51 – 8.50 μm. It should be noted that the presence of platinum near the track openings has affected the early measurement steps up to 0.50 μm, which have been excluded from Figure 6.

Two additional mounts etched respectively for 1 and 5 min were prepared for analysis, but no tracks were visible under the FIB-SEM. Therefore, additional experimental steps were performed to determine whether the etchant had penetrated the cores of the implanted tracks during these short etch times, but the resulting features were simply below the microscope resolution. The slightly etched grains were therefore removed from their epoxy mounts using a commercial paint stripper and annealed in aluminium tubes in a *Ratek Digital* Dry Block Heater at 400°C for 8 hours to remove any remaining unetched track damage. The loose monazite grains for each sample were then remounted by placing them polished-face down on double-sided tape before re-embedding in cold-setting *Struers* Epofix epoxy. The original polished surfaces were then re-etched in 6M HCl at 90°C for 75 min.

The rationale behind this etch-anneal-etch procedure (e.g. Green et al., 1978; Tamer & Ketcham, 2020) was that if the etchant had penetrated along the fission tracks during their initial 1 and 5 min etching schedule, removal of the highly reactive latent track core should make the track immune to subsequent thermal annealing, even though the etched cores were below the resolution of the SEM. The second round of etching would then enlarge these fission track cores to the length that had been initially etched.

Optical microscope images of the remounted monazite grains were captured and fission track lengths determined manually using *FastTracks* on 500 track measurements as described in Section 2.2. Table 5 and Figure 7 present the results of this etch-anneal-etch experiment performed on the two mounts. The results show that after the second 75 min etch, both mounts revealed implanted fission tracks that had survived the annealing step due to prior short etching. The average fission track lengths were 4.13 ± 0.04 μm and 4.04 ± 0.04 μm for the 5 and 1 min etch, respectively, which are indistinguishable from each other. The average bulk etching velocity between the two etching steps is calculated to be ~0.0019 μm/s (Tamer & Ketcham, 2020). The maximum lengths measured for each sample were 7.62 μm and 7.79 μm for the 5- and 1-min etch respectively. It was not possible to measure track widths accurately using this method.

3. Discussion

When viewed under the SEM, well-etched spontaneous fission track openings on (100) surfaces, parallel to the crystallographic b- and *c*-axes, are rhombic in shape (Figure 8a), as are those on surfaces cut perpendicular to the *c*-axis (Figure 8b). Track openings observed on the (010) plane have a more complex, elongated shape, as shown in Figure 8c. By contrast in apatite, track openings on the preferred prismatic faces parallel to the crystallographic *c*-axis form hexagonal shapes, strongly elongated in the *c*-axis direction. More regular hexagonal etch pits are found on basal surfaces perpendicular to the *c*-axis (Wagner & Van den Haute, 1992). Track etch pit shapes in both monazite and apatite reflect the underlying crystal symmetry.

Dimensions of the rhombic cross-sections of well-etched spontaneous fission tracks in both the Harcourt and Eldorado monazite are broadly similar, indicating the typical size of well-etched track openings under the etching conditions used. Electron microprobe analyses of these two monazites (Table 1) show differences in U, Th, Ca and light rare earth elements

(LREE) content, which is consistent with the known chemical variability of monazite (e.g. Clavier et al., 2011; Ruschel et al., 2012). However, it is not clear from this limited evidence what influence crystal chemistry may have on track etching or annealing kinetics.

Since monazite track etch pits on surfaces parallel and perpendicular to (100) are similar in appearance and symmetrical, so the form of the etch pits is more difficult to use as an identifier of surface orientation, unlike the case in apatite. Similarly, the orientation of the rhombic track openings does not provide an unambiguous indication of the direction of the crystallographic *c*-axis, again contrasting with apatite. However, the difficulty in distinguishing these two quite different orientations based on the track etching characteristics probably also implies that both will be similarly useful for counting fission tracks. Although not studied in detail, the form of track etch pits on a (010) surface (Figure 8c) do appear different to the other two orientations. At least for euhedral crystals, surfaces parallel to (100) are likely to be the most common.

The angular distribution experiment shows that in the first 60 min of etching fission tracks on (100) faces are revealed anisotropically relative to the *c*-axis (Fig 2a). The degree of anisotropy decreases progressively, however, so that after etching for 90 min, the angular distribution becomes isotropic (Fig 2b). On its own merit, this experiment suggests that monazite should be routinely etched for 90 min under the etchant conditions used to ensure tracks are revealed in all orientations. However, it was also evident that even after 60 min some grains were already strongly-etched and tracks eventually became too difficult to accurately measure in the later etching stages so some variability is apparent, possibly due to radiation damage or compositional effects. Jones et al. (2019) concluded that the optimal time for etching of fission tracks in the same monazite and using the 6M HCl etchant at 90°C was 75 min which also represented a compromise between grains showing different degrees of etching.

The anisotropic track measurements shown in Figure 2a were averaged across all grains measured, including many that had already reached fully isotropic etching by 60 min as well as others that had not. It is therefore concluded, in line with etching tracks in other variable etching rate minerals such as zircon and titanite (e.g. Gleadow et al., 1976; Gleadow, 1978), that the etching time for any particular monazite grain may need to be judged by the degree of etching of the tracks themselves. Etching for 75 min would fully reveal fission tracks to an isotropic distribution in most grains of this particular monazite. However, for some grains with higher concentrations of U and Th, it was apparent that tracks were already over-etched within this same etching time. These results support our earlier findings (Jones et al., 2019) for the Harcourt Granodiorite monazite that 2-3 mounts may need to be etched for different times over at least a range of 60 – 90 min to obtain a representative distribution of ages within the sample.

Results of the FIB-SEM experiments show firstly that etching of implanted ^{252}Cf fission tracks shows a general decrease in width along their length (Table 4, Fig 4). The 60-min control sample shows an overall decreasing width with increasing distance along the track. The dramatic drop-off in width for the one track recorded between 8.01 – 8.50 μm is likely due to it having been measured very close to its end. In both the 15 and 10 min experiments, a trend of decreasing track width along the track is observed.

It is evident that after 10 min etching well-defined tracks were revealed up to 7.00 μm in length. In both the 15 min and 60 min control sample, track lengths <7.00 μm account for ~97% of data for each experiment, suggesting that the etchant penetrated along most of the latent fission track lengths within 10 min. Weise et al. (2009) calculated the mean ranges of heavy and light ^{235}U fission fragments in monazite to be ~8.30 μm and 10.80 μm, respectively. These combine to give a total range for an average latent track of ~19 μm. The etchable range calculated for an equivalent confined fission track from a ^{252}Cf source in monazite is ~10 – 11 μm in length (Jones et al., 2021) suggesting an unetchable length deficit of up to 8 μm (~4 μm at each end). Taking this into account, the average etchable range for the heavy and light fission fragments in monazite would be ~4.30 and ~6.80 μm, respectively. The continuous etching of single ^{252}Cf tracks observed up to ~7 μm suggests that tracks formed from both the light and heavy fission fragments have reached their full etchable range within 10 min.

The 5 and 1 min etching experiments were also investigated using the FIB-SEM, but no tracks could be seen because their widths were not sufficient relative to the instrument resolution (~25 nm). However, the etch-anneal-etch experiments clearly demonstrated that the 6M HCl etchant did in fact penetrate and etch the fission tracks, even within very short etching times. Although no direct comparison can be made with the FIB-SEM measurements, as the widths could not be quantified, a number of observations can be made. The fact that the implanted fission tracks were still present following the etch-anneal-etch procedure indicates that the 6M HCl etchant had penetrated and removed the damaged cores of the implanted fission tracks more or less instantaneously (<1 min). From Figure 7 it is clear that fission track lengths measured in the 5 and 1 min etching experiments were etched to similar maximum lengths, but overall the distributions are shifted to shorter lengths compared to the control dataset.

The average length of well-etched and unannealed ^{252}Cf fission tracks from the 60 min control dataset is 4.96 ± 0.03 μm, which is significantly longer by ~0.92 μm than the average lengths for the 5 and 1 min etching experiments, which are 4.13 ± 0.04 μm and 4.04 ± 0.04 μm, respectively. The mean track length for the 5 min etch is slightly longer than that for the 1 min etch, although the difference is not significant at the 95% confidence level. Taken at face value, these mean and maximum length measurements suggest that at least the greater part of the etchable ranges of the latent fission tracks were penetrated by the etchant within the first few min.

A total of 69 and 60 measurements were recorded for tracks >5.01 μm in length for the 5 and 1 min experiments (Table 5), 13.8 and 12 % respectively. By contrast in the control sample, a total of 251 (50%) were recorded for tracks in the same range, out of a total number of 500 track measurements in each case. There is a dramatic decrease in the number of recorded tracks >5.01 μm in both experiments compared to the control sample. Furthermore, the relatively small increase in average lengths between the 1 and 5 min experiments implies that even with an extra 4 min, the etchant on average is only making gradual progress along the length of the track.

Based on the results of both the FIB-SEM and etch-anneal-etch experiments, it is estimated that the 6M HCl etchant at 90°C takes between 5 – 10 min to fully penetrate the etchable lengths of implanted ^{252}Cf fission tracks in monazite. The isothermal annealing experiment of Jones et al. (2019), found that implanted ^{252}Cf fission tracks showed an average length reduction of 4% after 1 hour when exposed to temperatures of 90°C. Taking both of these observations into account suggests that the implanted ^{252}Cf fission tracks would experience no more than ~1% thermal annealing before becoming fully etched along their etchable range, and therefore immune to further annealing. It should also be noted that all the Cf track measurements in this study were performed on fission tracks implanted at dips of 30° and an azimuth of ~0° to the crystallographic c-axis. This is a relatively slow etching orientation based on the angular distribution experiment for randomly oriented spontaneous tracks, making the estimates here the maximum times for the etchant to fully penetrate the length of most fission tracks in monazite.

5. Implications

This study presents the results of a series of experiments on two monazites, from the Harcourt Granodiorite and an alluvial deposit from Beechworth in Victoria, aimed at further elucidating their fission track etching properties. We make the following observations:

1) SEM images of tracks etched on (100) surfaces in monazite show that well-etched spontaneous fission track openings are rhombic in shape. This reflects the underlying crystal symmetry, with average dimensions of 0.81 ± 0.20 μm and 0.73 ± 0.26 μm for the maximum diameters Dpc and Dpb, respectively. Very similar rhombic track openings are observed on surfaces parallel to the (100) face and perpendicular to the c-axis making it difficult to differentiate between the two. Both orientations are probably equally suitable for fission track counting.

This is the peer-reviewed, final accepted version for American Mineralogist, published by the Mineralogical Society of America.
The published version is subject to change. Cite as Authors (Year) Title. American Mineralogist, in press.
DOI: https://doi.org/10.2138/am-2022-8002. http://www.minsocam.org/

2) Track etching of spontaneous fission tracks on monazite (100) faces is initially anisotropic with tracks etching faster at azimuths of 90° to the crystallographic *c*-axis than those oriented closer to 0°. As etching continues for up to 90 min, this anisotropy progressively disappears. This observation complements the findings of Jones et al. (2019), where a step-etch experiment suggested that fission tracks in monazite are well-etched after about 75 min. However, the etching rate appears be variable and to increase with higher U and Th content. Considering the abundance of these elements in monazite this is probably in large part due to radiation damage effects, as also observed in zircon and titanite. Etching for 75 – 90 min can therefore lead to significant over-etching of grains with higher U and Th. Given this variability, it may be necessary to prepare multiple mounts etched for different times in the 60-90 min range to obtain a representative distribution of ages within a sample.

3) Ion milling using a FIB-SEM to expose successive sections along collimated ^{252}Cf fission tracks shows that the diameters of the tracks taper from the surface to their terminations. The average diameters of the tracks decrease to roughly half of their near-surface values towards their ends. The longest track measured had a length of 8.0-8.5 µm in the 60 min control sample and appears to be close to the maximum etchable range for a light fission fragment. The smallest track diameters were measured at lengths of 5.5-6.0 µm and 6.5-7.0 µm for two shorter etching times of 15 and 10 min respectively, but both these measurements are about 25 nm and close to the resolution of the SEM. This suggests that the latent track cores have been etched to even greater lengths and this is confirmed by several tracks being observed in the 15 min sample up to a maximum of >8.5 µm, although their diameters could not be measured. These results suggest that the

etchant has already penetrated along the full etchable range of at least some of the Cf tracks by these relatively short etching times, long before they are observable optically. It is also concluded that the FIB-SEM technique has considerable potential for studies of track etching in other minerals.

4) Results of etch-anneal-etch experiments show that the 90°C 6M HCl etchant penetrates close to the full etchable range of the ^{252}Cf fission tracks within an even shorter etching time of 5 min, and possibly 1 min. The resulting etch channels were below the resolution of the FIB-SEM experiments and so are estimated to be less than ~25 nm in diameter. Subsequent etching following the annealing step to remove any unetched radiation damage showed that the first short etching steps had penetrated to lengths of 7-8 µm. The isothermal annealing experiment of Jones et al. (2019), suggests that ~4% track shortening would occur in 60 min, therefore after ~15 min any thermal annealing during etching should be no more than ~1%. The effect may be even less if full etchant penetration has occurred by 5 min.

Acknowledgements

We thank Abaz Alimanovíc and Ling Chung for assistance in the laboratory, and Graham Hutchinson for SEM analysis and imagery. Sergey Rubanov of the Bio21 Institute, University of Melbourne is also thanked for training and assistance with the FIB-SEM. SJ acknowledges funding from the Australian Government through the Research Training Program (RTP) Scholarship. The Melbourne thermochronology laboratory is supported by the AuScope Program funded under the National Collaborative Research Infrastructure Strategy (NCRIS).

We thank Murat Tamer, Ewald Hejl and an anonymous reviewer for their thorough and constructive reviews, which improved the manuscript.

References

Clavier, N., Podor, R., & Dacheux, N. (2011). Crystal Chemistry of the Monazite Structure. *Journal of the European Ceramic Society*, *31*(6), 941–976. https://doi.org/10.1016/j.jeurceramsoc.2010.12.019

Clemens, J.D. (2018). Granitic magmas with I-type affinities , from mainly metasedimentary sources : the Harcourt batholith of southeastern Australia. *Contributions to Mineralogy and Petrology*, *173*(11), 1–20. https://doi.org/10.1007/s00410-018-1520-z

Donelick, R.A., O'Sullivan, P.B., & Ketcham, R. A. (2005). Apatite Fission-Track Analysis. *Reviews in Mineralogy and Geochemistry*, *58*(1), 49–94. https://doi.org/10.2138/rmg.2005.58.3

Gleadow, A.J.W. (1978). Anisotropic and Variable Track Etching Characteristics in Natural Sphenes. *Nuclear Track Detection*, *2*, 105–117.

Gleadow, A.J.W., Gleadow, S. J., Frei, S., Kohlmann, F., & Kohn, B. P. (2009). Automated analytical techniques for fission track thermochronology. *Geochimica et Cosmochimica Acta Supplement*, *73*, A441.

Gleadow, A.J.W., Hurford, A. J., & Quaife, R. D. (1976). Fission Track Dating of Zircon: Improved Etching Techniques. *Earth*, *33*, 273–276.

Gleadow, A., Kohn, B., & Seiler, C. (2019). The Future of Fission-Track Thermochronology. In M. Malusà & Fitzgerald P (Eds.), *Fission-Track Thermochronology and its Application to Geology* (pp. 77–92). Springer.

Green, P.F., Bull, R.K., & Durrani, S.A. (1978). Particle identification from track-etch rates in minerals. *Nuclear Instruments and Methods*, *157*(1), 185–193.

Jones, S., Gleadow, A., & Kohn, B. (2021). Thermal Annealing of Implanted 252Cf Fission-Tracks in Monazite. *Geochronology*, *3*, 89–102.

Jones, S., Gleadow, A., Kohn, B., & Reddy, S.M. (2019). Etching of fission tracks in monazite : An experimental study. *Terra Nova*, (Special Issue-Thermo2018), 1–10. https://doi.org/10.1111/ter.12382

Kohn, B.P., Chung, L., & Gleadow, A.J.W. (2019). Fission-Track Analysis: Field Collection, Sample Preparation and Data Acquisition. In M. G. Malusà & P. G. Fitzgerald (Eds.), *Fission-Track Thermochronology and its Application to Geology* (pp. 25–48). Springer Textbooks in Earth Sciences, Geography and Environment. https://doi.org/https://doi.org/10.1007/978-3-319-89421-8

Price, P.B., & Walker, R.M. (1962). Chemical etching of charged-particle tracks in solids. *Journal of Applied Physics*, *33*(12), 3407–3412. https://doi.org/10.1063/1.1702421

Ruschel, K., Nasdala, L., Kronz, A., Hanchar, J.M., Többens, D.M., Škoda, R., Finger, F., & Möller, A. (2012). A Raman spectroscopic study on the structural disorder of monazite–(Ce). *Mineralogy and Petrology*, *105*(May 2012), 41–55. https://doi.org/10.1007/s00710-012-0197-7

Shukoljukov, J.A., & Komarov, A.N. (1970). Tracks of uranium fission in monazite (in Russian). In *Bulletin of the Commission for the Determination of the Absolute Age of Geological Formations* (pp. 20–26). Moscow: Akad. Nauk. USSR.

Sullivan, C.J. (1947). *Record 1947/10: Geology and mineral resources of the Murray Valley Region*. Australia. Bureau of Mineral Resources, Geology and Geophysics.

Tamer, M.T., & Ketcham, R.A. (2020). The along-track etching structure of fission tracks in apatite: Observations and implications. *Chemical Geology*, *553*(July), 119809.

https://doi.org/10.1016/j.chemgeo.2020.119809

Wagner, G.A., & Van den Haute, P. (1992). *Fission-Track Dating* (2nd ed.). Stuttgart: Solid Earth Sciences Library Vol.6, Kluwer Academic Publishers.

Weise, C., van den Boogaart, K.G., Jonckheere, R., & Ratschbacher, L. (2009). Annealing kinetics of Kr-tracks in monazite: Implications for fission-track modelling. *Chemical Geology*, *260*(1–2), 129–137. https://doi.org/10.1016/j.chemgeo.2008.12.014

Wirth, R. (2009). Focused Ion Beam (FIB) combined with SEM and TEM : Advanced analytical tools for studies of chemical composition , microstructure and crystal structure in geomaterials on a nanometre scale. *Chemical Geology*, *261*(3–4), 217–229. https://doi.org/10.1016/j.chemgeo.2008.05.019

Young, R.J., & Moore, M.V. (2005). DUAL-BEAM (FIB-SEM) SYSTEMS Techniques and Automated Applications. In L. A. Giannuzzi & F. A. Stevie (Eds.), *Introduction to Focused Ion Beams. Instrumentation, Theory, Techniques and Practice* (pp. 247–268). New York: Springer Science & Business Media.

List of Figure Captions

Figure 1. (a) Typical monazite crystal with Miller Indices and crystallographic axes. (b) Surface plane for crystals oriented on their (100) face and typical shape of spontaneous track opening. Dpc = diameter of track opening parallel to the crystallographic c-axis and Dpb = diameter of track opening parallel to the b-axis.

Figure 2. (a) Angular distribution of spontaneous fission tracks after etching times of 20, 40 and 60 min. During these etching times, tracks are revealed anisotropically, with tracks with an azimuth 90° to the crystallographic *c*-axis revealed first. Numbers in brackets represent

the number of tracks measured for the respective etching time. (b) Angular distribution of spontaneous fission tracks after etching for 90 min. Tracks are revealed more uniformly across different angles to the *c*-axis after this longer etching time. (c) The ratio of the number of tracks from 75-90° to the c-axis relative to the number from 0-15° for each time step of the experiment showing the convergence towards isotropic etching of the tracks. The values adjacent to the points represent the average spontaneous semi-track length (μm) for each etching time.

Figure 3. (a) Diagram illustrating the FIB-SEM setup. The FIB component is used to progressively mill slices of the monazite crystal and the SEM beam is used for imaging and measuring the track widths and depths. Note the angle of the sample and both beams have been rotated for ease of illustration. Usually, the specimen would be tilted 52° and SEM beam positioned vertically at 90°. Diagram not to scale. (b) SEM image of a milled monazite section with implanted ^{252}Cf fission tracks. Etched tracks can be seen on the crystal surface and milled sub-surface. White arrow shows direction of crystallographic *c*-axis on original surface.

Figure 4. Average ^{252}Cf fission track width at increasing distance along the etched track lengths for different etching times of 60 (control), 15 and 10 min. All experiments display an overall decreasing width trend, with a maximum length of <9.00 μm. The presence of platinum near the track openings has affected the early measurement steps of the 60 min control sample up to ~1.00 μm (dotted blue line) and has been excluded from the rest of the analyses.

Figure 5. (a) SEM image of a milled plane demonstrating platinum deposition on the monazite surface and penetrating into the track opening. (b) Schematic cross-section illustrating platinum deposition into the track opening, impairing measurements of near surface tracks in the early milling steps.

Figure 6. Percentage of ^{252}Cf fission tracks measured between lengths 1 – 9 μm. Measurements <1 μm were excluded due to platinum deposition near the track openings.

Figure 7. ^{252}Cf fission track length distributions using the etch-anneal-etch procedure for the 5 and 1 min experiments. The control dataset is the ^{252}Cf fission track length distribution from Section 2.3 of Jones et al. (2019). The overall track length distributions for the 5 and 1 min experiments after annealing and re-etching for 75 min are shorter than the control sample, but the maximum lengths revealed are similar in all cases.

Figure 8. Images from Harcourt Granodiorite monazite. (a) SEM image of well-etched spontaneous fission track openings on the (100) pinacoid face. Enlarged image taken at 19000 x magnification. (b) SEM Image of well-etched spontaneous fission track openings on a surface perpendicular to the crystallographic *c*-axis. Enlarged image taken at 3500 x magnification. (c) SEM image of spontaneous fission track openings on the (010) pinacoid. Enlarged image taken at 3700 x magnification. Arrows indicate directions of crystallographic axes relative to the etched surface. Scale bar is 1 μm in all images.

Tables

Table 1. Average chemical composition of Harcourt Granodiorite and Eldorado Dredge monazite (± 2σ errors).

	Harcourt*	**Eldorado****
Element	**Mean Wt%**	**Mean Wt%**
SiO_2	1.63 ± 0.04	1.01 ± 0.15
P_2O_5	27.37 ± 0.15	27.24 ± 0.24
CaO	0.45 ± 0.02	1.15 ± 0.14
Y_2O_3	2.39 ± 0.05	2.53 ± 0.13
La_2O_3	14.13 ± 0.17	8.72 ± 0.71
Ce_2O_3	28.54 ± 0.26	25.80 ± 0.63
Pr_2O_3	4.45 ± 0.11	3.40 ± 0.07
Nd_2O_3	10.61 ± 0.13	12.53 ± 0.30
Sm_2O_3	1.80 ± 0.08	3.58 ± 0.25
Gd_2O_3	1.34 ± 0.08	2.06 ± 0.09
ThO_2	6.31 ± 0.11	8.43 ± 0.84
UO_2	0.50 ± 0.04	0.81 ± 0.08
Al_2O_3		0.00 ± 0.001
FeO		0.01 ± 0.002
SO_3		0.02 ± 0.002
PbO		0.19 ± 0.02
DY_2O_3		0.96 ± 0.05
Yb_2O_3		0.15 ± 0.01
Er_2O_3		0.11 ± 0.01
Tb_2O_3		0.28 ± 0.02
Sum Ox%	**99.52**	**98.98**

* Measurements on 81 grains made with a Cameca SX50 electron microprobe using a 10 μm beam width, 50 KeV beam current, 25 KV accelerating voltage and take off angle of 40°.

** Measurements made on 16 grains with a Jeol JXA-8530F electron microprobe using a 5 μm beam width, 300 nA beam current and 15 KV accelerating voltage

Table 2. Details of the various etching experiments in this study. All samples were etched in 6M HCl at 90°C.

Experiment	Track Type	Etching Time (Min)	Etch Type	Method of Measurement	Sample Location
Section 2.1	Spontaneous ^{238}U	75	Continuous	*FastTracks* and SEM	Harcourt, Beechworth
Section 2.2	Spontaneous ^{238}U	20-40-60-90	Step-etch	*FastTracks*	Harcourt
Section 2.3	Implanted ^{252}Cf	10, 15, 60	Continuous	FIB-SEM	Harcourt
		1, 5, 60	Etch-anneal-etch	*FastTracks*	Harcourt

Table 3. Average spontaneous fission track etch pit dimensions Dpc and Dpb (± 1 standard error) for Harcourt Granodiorite and Eldorado Dredge monazites.

Optical *(FastTracks)* Measurements

	Harcourt Granodiorite		Eldorado		All Analyses	
	Dpc (µm)	**Dpb (µm)**	**Dpc (µm)**	**Dpb (µm)**	**Dpc (µm)**	**Dpb (µm)**
Average	0.82 ± 0.01	0.79 ± 0.01	0.84 ± 0.01	0.78 ± 0.01	0.83 ± 0.01	0.78 ± 0.01
Standard Deviation	0.17	0.14	0.20	0.21	0.18	0.18
Count	386	394	279	311	665	705

SEM Measurements

	Harcourt Granodiorite		Eldorado		All Analyses	
	Dpc (µm)	**Dpb (µm)**	**Dpc (µm)**	**Dpb (µm)**	**Dpc (µm)**	**Dpb (µm)**
Average	0.77 ± 0.03	0.80 ± 0.04	0.85 ± 0.02	0.67 ± 0.02	0.81 ± 0.02	0.73 ± 0.02
Standard Deviation	0.22	0.33	0.18	0.15	0.20	0.26
Count	65	65	65	65	130	130

SEM conditions were 15 Kv accelerating voltage and working distance of ~10 mm

Table 4. Etched track widths (± 1 standard error) of Implanted ^{252}Cf fission tracks at different length intervals from the surface after etching for 60, 15 and 10 min.

60 Minute Etch - Control

Length Interval (µm)	Average Semi-Track Width (nm)	Track Count	% of Total Tracks
Track Opening	*299.6 ± 17.3*	*30*	*5.7*
0.01 - 0.50	*330.4 ± 24.8*	*10*	*1.9*
0.51 - 1.00	*379.0 ± 11.5*	*57*	*10.8*
1.01 - 1.50	407.3 ± 9.1	73	13.8
1.51 - 2.00	416.9 ± 8.1	49	9.3
2.01 - 2.50	434.0 ± 13.6	52	9.8
2.51 - 3.00	393.9 ± 11.3	53	10.0
3.01 - 3.50	369.6 ± 13.6	41	7.8
3.51 - 4.00	359.1 ± 11.6	42	7.9
4.01 - 4.50	341.5 ± 11.9	30	5.7
4.51 - 5.00	307.5 ± 22.4	27	5.1
5.01 - 5.50	300.0 ± 14.6	18	3.4
5.51 - 6.00	284.1 ± 22.3	14	2.6
6.01 - 6.50	291.1 ± 21.0	13	2.5
6.51 - 7.00	301.5 ± 23.4	8	1.5
7.01 - 7.50	254.5 ± 34.2	8	1.5
7.51 - 8.00	273.4 ± 40.7	3	0.6
8.01 - 8.50	164.3	1	0.2
8.51 - 9.00			
Average	**329.9 ± 14.1**		
Total		**529**	**100.0**

15 Minute Etch

Length Interval (µm)	Average Semi-Track Width (nm)	Track Count	% of Total Tracks
Track Opening	*104.1 ± 11.2*	*2*	*0.9*
0.01 - 0.50	*83.9 ± 6.3*	*29*	*13.4*
0.51 - 1.00	68.3 ± 4.5	32	14.8
1.01 - 1.50	57.2 ± 4.1	38	17.6
1.51 - 2.00	63.2 ± 5.9	23	10.6
2.01 - 2.50	63.9 ± 5.8	25	11.6
2.51 - 3.00	60.6 ± 9.1	15	6.9
3.01 - 3.50	64.1 ± 6.5	15	6.9
3.51 - 4.00	60.0 ± 8.3	13	6.0
4.01 - 4.50	52.7 ± 8.4	9	4.2
4.51 - 5.00	38.1 ± 1.8	5	2.3
5.01 - 5.50	30.2	1	0.5
5.51 - 6.00	25.0	1	0.5
6.01 - 6.50			
6.51 - 7.00	**	2	0.9
7.01 - 7.50	**	5	2.3
7.51 - 8.00			
8.01 - 8.50			
8.51 - 9.00	**	1	0.5
Average	**55.6 ± 6.7**		
Total		**216**	**100.0**

10 Minute Etch

Length Interval (µm)	Average Semi-Track Width (nm)	Track Count	% of Total Tracks
Track Opening	*73.2*	*1*	*0.2*
0.01 - 0.50	*47.4 ± 2.2*	*41*	*7.4*
0.51 - 1.00	43.8 ± 1.4	65	11.8
1.01 - 1.50	39.9 ± 1.6	67	12.1
1.51 - 2.00	39.3 ± 1.3	59	10.7
2.01 - 2.50	35.7 ± 1.0	69	12.5
2.51 - 3.00	33.7 ± 1.2	58	10.5
3.01 - 3.50	32.1 ± 1.0	44	8.0
3.51 - 4.00	31.6 ± 1.2	49	8.9
4.01 - 4.50	28.4 ± 1.1	40	7.2
4.51 - 5.00	28.4 ± 1.3	19	3.4
5.01 - 5.50	26.6 ± 1.5	29	5.2
5.51 - 6.00	29.0 ± 2.2	8	1.4
6.01 - 6.50	32.0 ± 3.6	2	0.4
6.51 - 7.00	23.1 ± 3.9	2	0.4
7.01 - 7.50			
7.51 - 8.00			
8.01 - 8.50			
8.51 - 9.00			
Average	**33.65 ± 1.41**		
Total		**553**	**100.0**

** Track observed but not measured due to poor focussing on the SEM image
Figures in italics show measurements affected by Pt deposition near the track openings

Table 5. Etched lengths of Implanted ^{252}Cf fission tracks for the etch-anneal-etch experiments.

60 Minute Etch (Control Sample)			**5 + 75 Min Etch**			**1 +75 Min Etch**		
Length Interval (μm)	**Total Count of Tracks**	**Total % of Tracks**	**Length Interval (μm)**	**Total Count of tracks**	**Total % of Tracks**	**Length Interval (μm)**	**Total Count of Tracks**	**Total % of Tracks**
0.00 - 0.50	0	0.00	0.00 - 0.50	0	0.0	0.00 - 0.50	0	0.0
0.51 - 1.00	0	0.00	0.51 - 1.00	0	0.0	0.51 - 1.00	0	0.0
1.01 - 1.50	0	0.00	1.01 - 1.50	0	0.0	1.01 - 1.50	0	0.0
1.51 - 2.00	0	0.00	1.51 - 2.00	0	0.0	1.51 - 2.00	0	0.0
2.01 - 2.50	0	0.00	2.01 - 2.50	2	0.4	2.01 - 2.50	7	1.4
2.51 - 3.00	3	0.6	2.51 - 3.00	31	6.2	2.51 - 3.00	33	6.6
3.01 - 3.50	9	1.8	3.01 - 3.50	89	17.8	3.01 - 3.50	105	21.0
3.51 - 4.00	41	8.2	3.51 - 4.00	117	23.4	3.51 - 4.00	117	23.4
4.01 - 4.50	87	17.4	4.01 - 4.50	109	21.8	4.01 - 4.50	105	21.0
4.51 - 5.00	109	21.8	4.51 - 5.00	83	16.6	4.51 - 5.00	73	14.6
5.01 - 5.50	133	26.6	5.01 - 5.50	46	9.2	5.01 - 5.50	31	6.2
5.51 - 6.00	81	16.2	5.51 - 6.00	12	2.4	5.51 - 6.00	17	3.4
6.01 - 6.50	31	6.2	6.01 - 6.50	7	1.4	6.01 - 6.50	7	1.4
6.51 - 7.00	6	1.2	6.51 - 7.00	3	0.6	6.51 - 7.00	1	0.2
7.01 - 7.50	0	0.00	7.01 - 7.50	0	0.0	7.01 - 7.50	3	0.6
7.51 - 8.00	0	0.00	7.51 - 8.00	1	0.2	7.51 - 8.00	1	0.2
Total	**500**	**100**		**500**	**100**		**500**	**100**

Data for the control sample is from the Isothermal Annealing Experiment of Jones et al. (2019) based on 500 measurements.

Figures

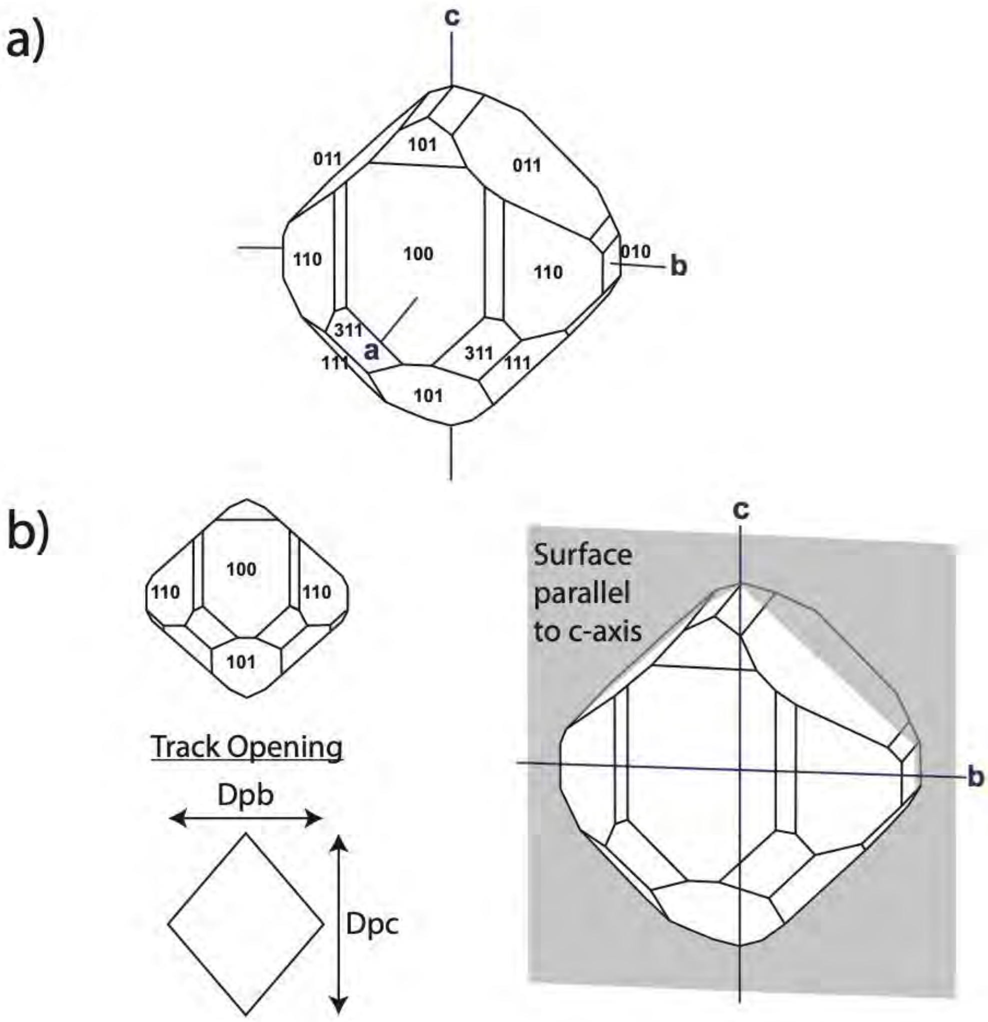

Figure 1 (above)

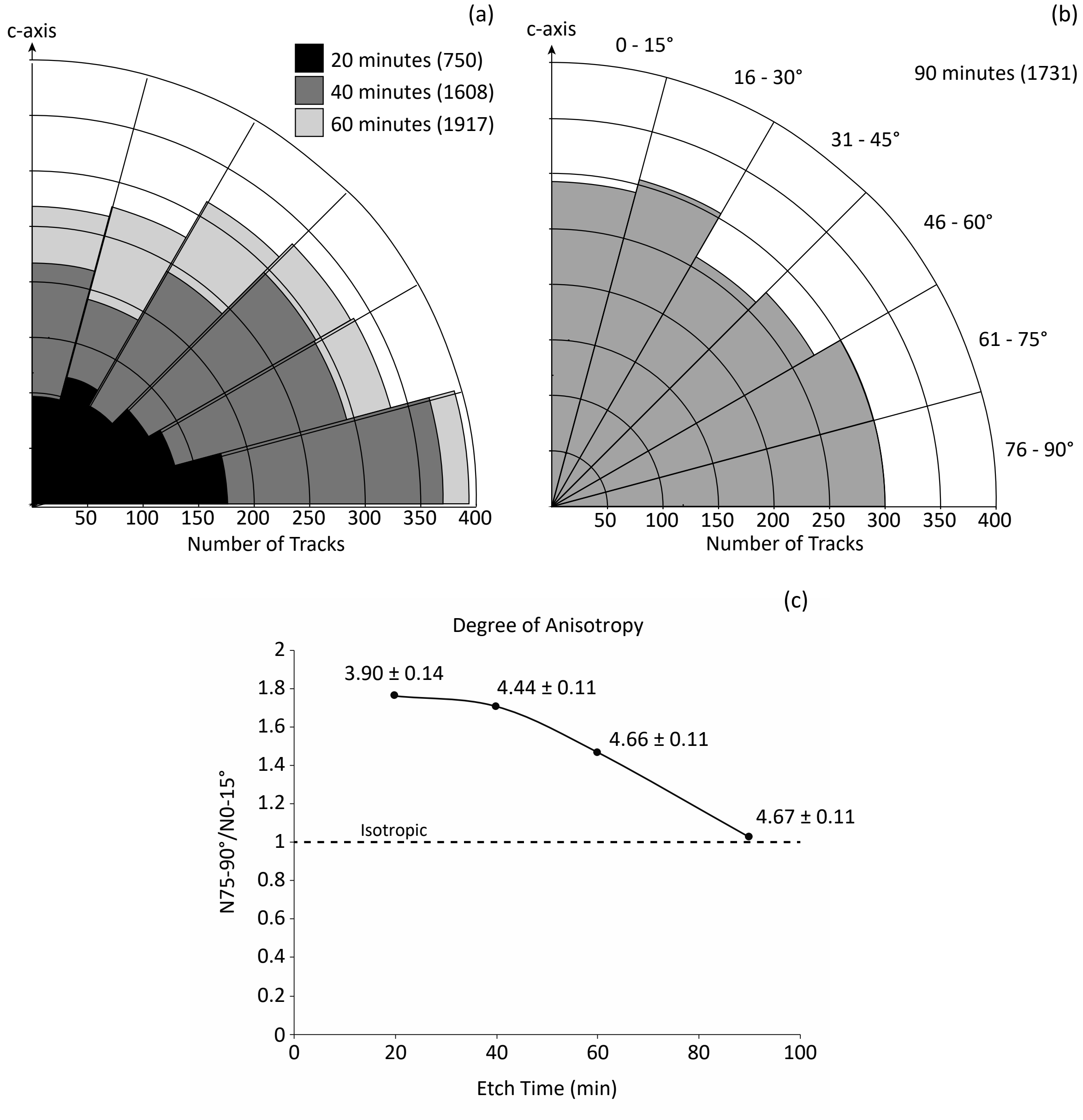

Figure 2 (above)

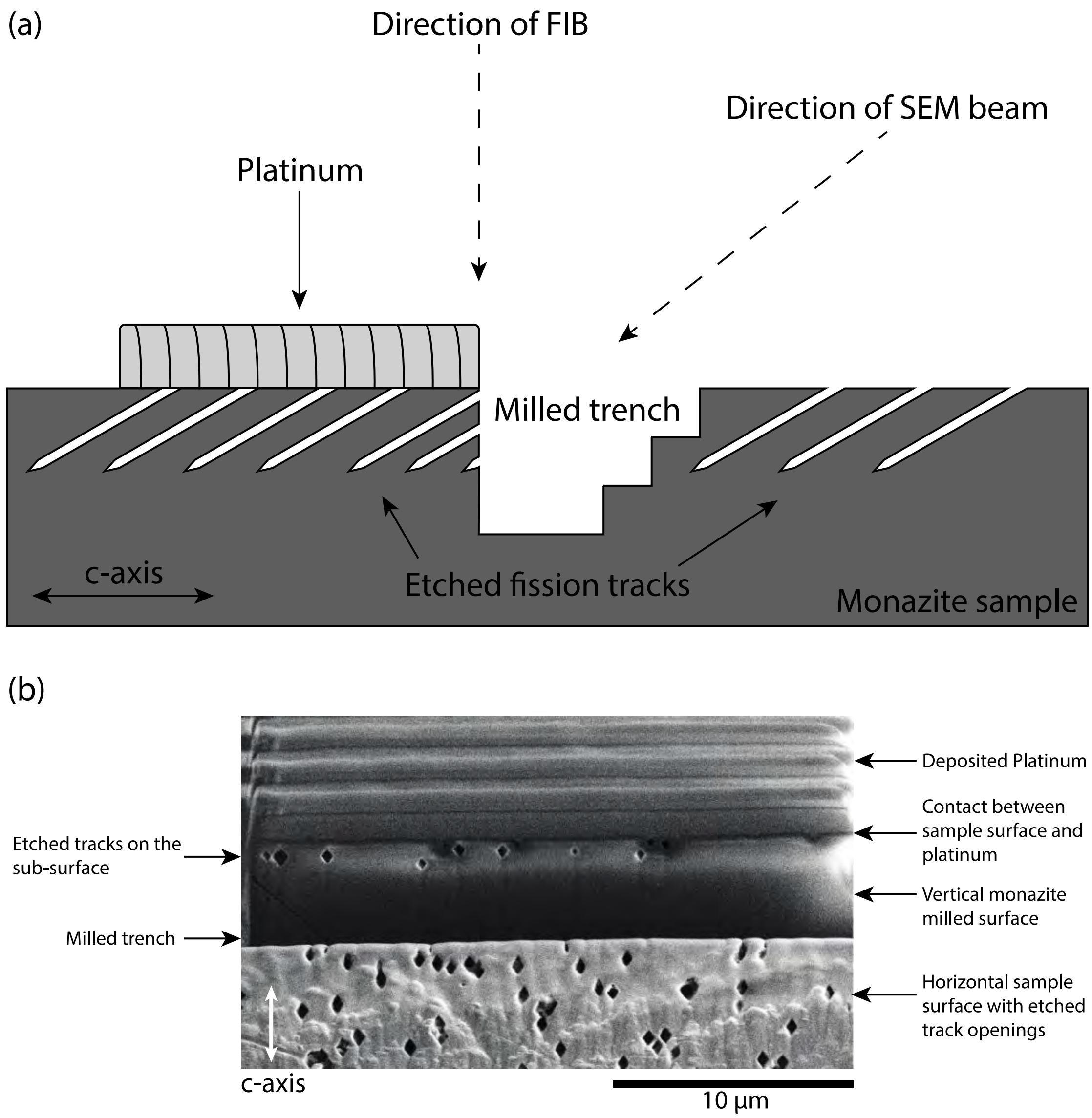

Figure 3 (above)

This is the peer-reviewed, final accepted version for American Mineralogist, published by the Mineralogical Society of America.
The published version is subject to change. Cite as Authors (Year) Title. American Mineralogist, in press.
DOI: https://doi.org/10.2138/am-2022-8002. http://www.minsocam.org/

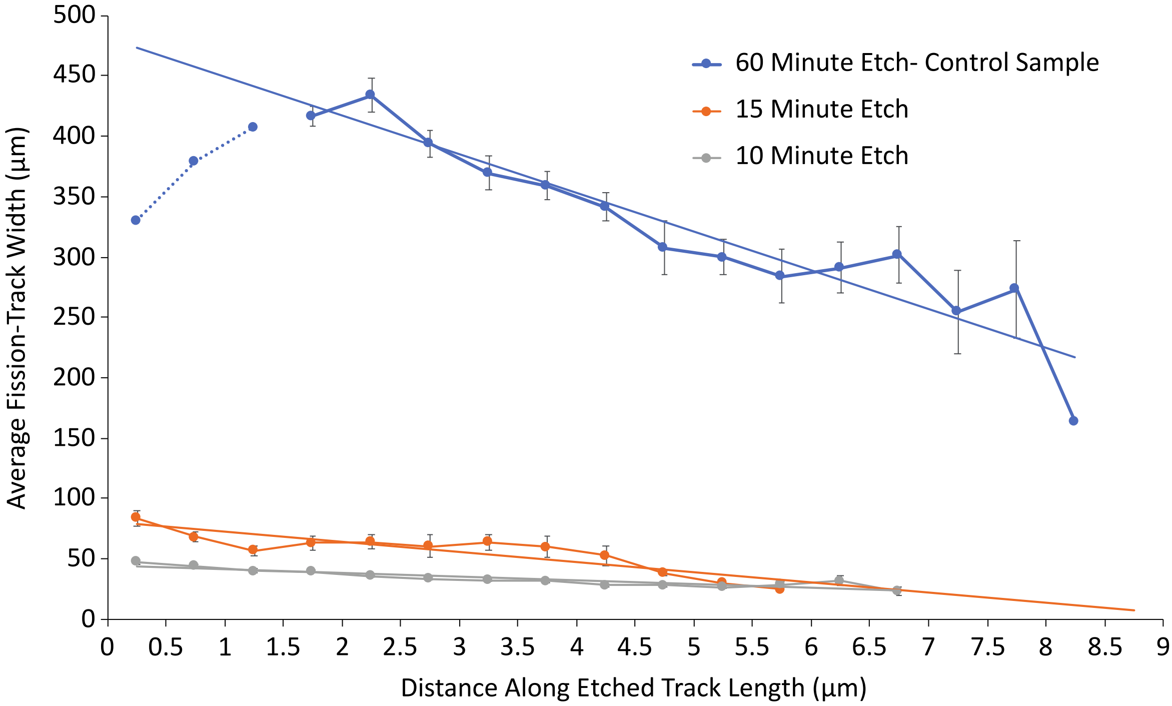

Figure 4 (above)

DOI: https://doi.org/10.2138/am-2022-8002. http://www.minsocam.org/

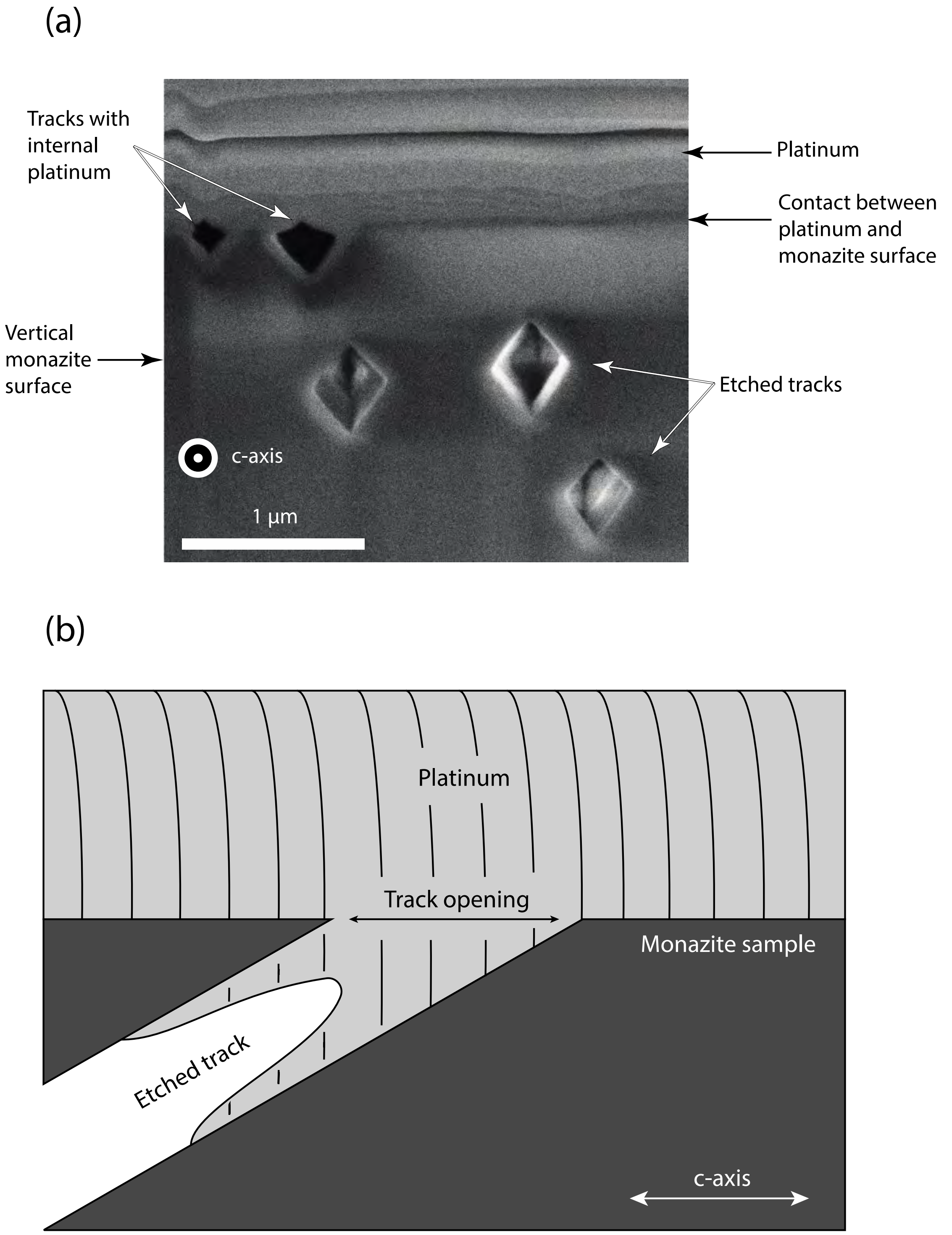

Figure 5 (above)

This is the peer-reviewed, final accepted version for American Mineralogist, published by the Mineralogical Society of America.
The published version is subject to change. Cite as Authors (Year) Title. American Mineralogist, in press.
DOI: https://doi.org/10.2138/am-2022-8002. http://www.minsocam.org/

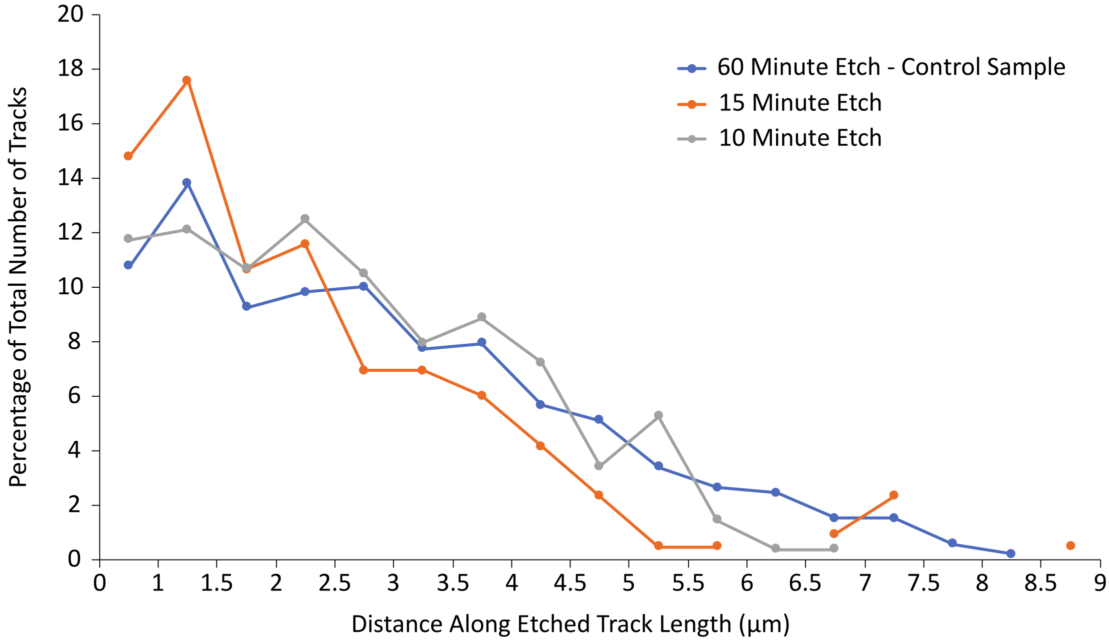

633

634 Figure 6 (above)

635

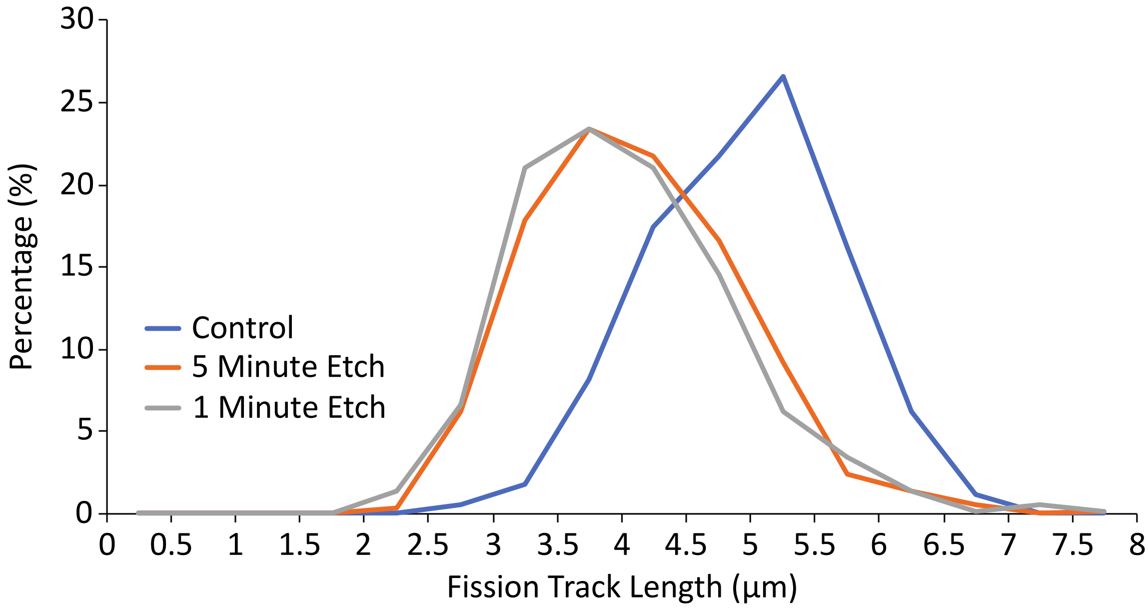

636

637 Figure 7 (above)

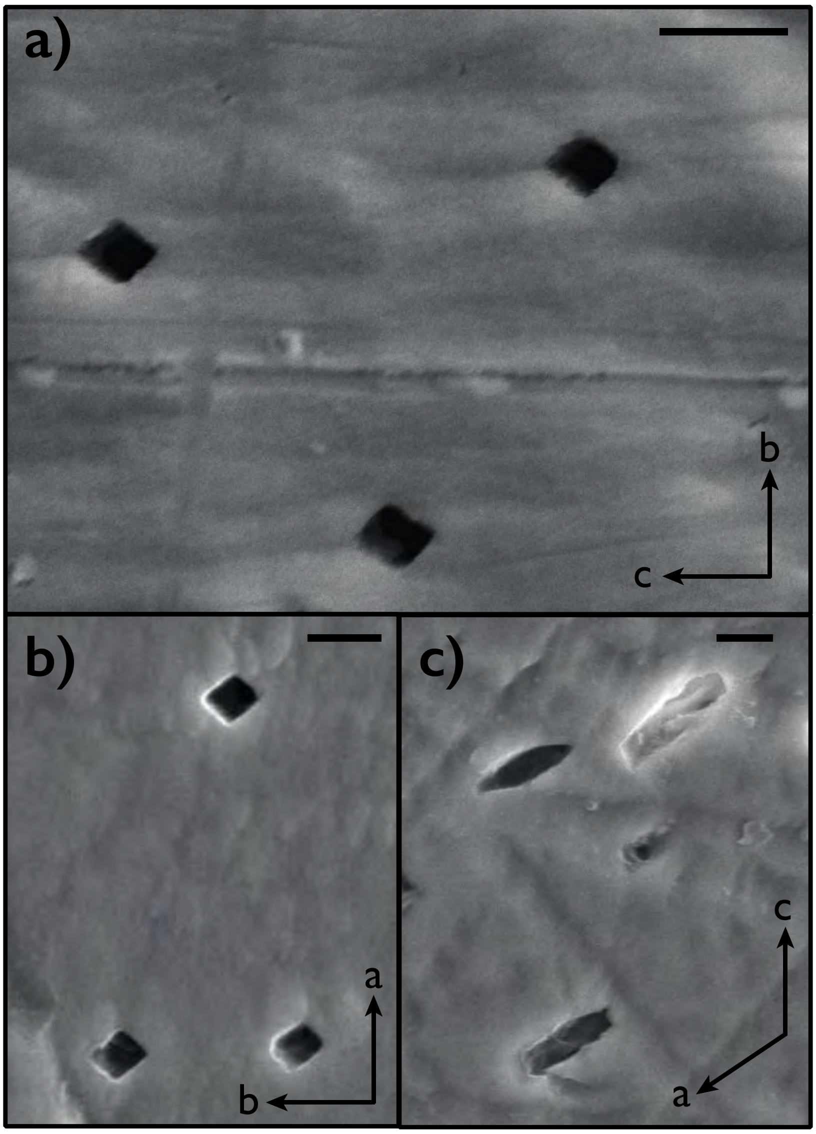

638

639 Figure 8 (above)